

# Forward–backward semiclassical dynamics for quantum fluids using pair propagators: Application to liquid *para*-hydrogen

Akira Nakayama

*Department of Chemistry, University of Illinois, Urbana, Illinois 61801*

Nancy Makri<sup>a)</sup>

*Department of Chemistry and Physics, University of Illinois, Urbana, Illinois 61801*

(Received 27 June 2003; accepted 29 July 2003)

Forward–backward semiclassical dynamics (FBSD) methods are emerging as a practical way of simulating dynamical processes in large quantum systems. In this paper we develop a pair-product approximation to the coherent state density. This form is accurate at low temperatures, enhancing significantly the convergence of Monte Carlo methods and thus allowing the simulation of quantum fluids. The scheme is applied to the calculation of velocity autocorrelation function of liquid *para*-hydrogen at several thermodynamic state points (between  $T=14$  K and  $T=25$  K). The results of the forward–backward semiclassical method with the pair-product approximation to the coherent state density exhibit good agreement with experimental measurements and other theoretical calculations. These calculations demonstrate that the FBSD method, in conjunction with an accurate representation of the coherent state density, allows an accurate description of dynamical processes in condensed phase systems at low temperatures where quantum mechanical effects play a significant role. © 2003 American Institute of Physics. [DOI: 10.1063/1.1611473]

## I. INTRODUCTION

The detailed understanding of quantum dynamical processes for polyatomic systems remains a challenging problem of much current interest. A complete and direct treatment of the dynamics for large systems using basis set methods requires storage of multidimensional wave functions and computational effort that grows exponentially with the number of degrees of freedom. These methods are therefore restricted to systems with only a few degrees of freedom. Another approach to quantum dynamics for large systems is based on Feynman's path integral formulation.<sup>1,2</sup> This method is, however, still prohibitive at long times because it involves evaluating a multidimensional integral of a highly oscillatory function. In spite of considerable progress using variations of filtering schemes,<sup>3–6</sup> Monte Carlo path integral integration methods generally fail when applied to oscillatory integrands due to uncontrolled phase cancellation. The so-called “sign problem” is also prevalent in fermion equilibrium path integral calculations.<sup>7</sup>

Time-dependent semiclassical theory<sup>8,9</sup> provides one of the viable alternatives for approximating quantum dynamical quantities and offers a potentially practical way for adding quantum mechanical effects to classical molecular dynamics simulations. The semiclassical approximation is based on classical trajectories and their stability properties, which can be obtained by inexpensive calculations even for very large systems.<sup>10</sup> These characteristics make semiclassical methods very appealing, as they can account for important quantum mechanical features of a system, while offering an intuitive understanding of dynamical processes.<sup>11–14</sup> In recent years,

the semiclassical method has experienced a rebirth of interest with the development of semiclassical initial value representations (SC-IVR)<sup>11,15–27</sup> which circumvent the troublesome “root search” problem of the original formulation. Numerical calculations exploiting these advances have demonstrated the ability of the semiclassical approximation to provide an accurate description of essentially all types of quantum effects in chemical dynamics,<sup>20,27–29</sup> and a number of successful applications to polyatomic molecules have been presented.<sup>26,27,30–38</sup> To date, the highly oscillatory character of the semiclassical integrand remains the main drawback of semiclassical methods, preventing integration by Monte Carlo methods in condensed phase systems. This situation is yet another manifestation of the sign problem discussed in the previous paragraph. We note, however, that significant progress has been reported through the introduction of filtering factors<sup>39</sup> and (in the case of the flux correlation function) the use of a symmetrized form with a smoother integrand.<sup>40</sup>

Forward–backward semiclassical dynamics (FBSD) methods,<sup>41–59</sup> originally developed in the context of influence functionals,<sup>41,42</sup> have recently emerged as a way of alleviating the problem associated with the oscillatory semiclassical phase. This idea is implemented by combining the forward and backward propagation steps that appear in ensemble-averaged quantities into a single time evolution whose dynamics are approximated by the semiclassical method. The semiclassical propagator constitutes the stationary phase limit of the fully quantum mechanical path integral description of the dynamics. The forward–backward treatment is equivalent to approximating an additional integral (that associated with the trajectory coordinates at the end of the forward evolution step) by the stationary phase method for all (or just some) degrees of freedom. By doing so, the

<sup>a)</sup>Electronic mail: nancy@makri.scs.uiuc.edu

oscillations originating from time propagation are minimized and the resulting integrand is sufficiently smooth, allowing evaluation by Monte Carlo techniques. The neglect of interference between distinct forward and backward trajectories implies that at least some aspects of quantum interference will be lost. Generalized forward-backward treatments<sup>57</sup> make use of a filtering factor with an adjustable weight, thereby allowing a partial cancellation of the semiclassical interference term. These developments hold promise for treating molecular systems with tens of atoms via semiclassical techniques.

To date, methods that completely eliminate the semiclassical phase provide the only practical choice for simulating condensed phase systems with several hundreds of coupled degrees of freedom. These include the Wigner method,<sup>60,61</sup> which has been rederived<sup>62,63</sup> by linearizing the semiclassical initial value representation of a time correlation function, and the derivative-FBSD method developed in our group.<sup>45,46</sup> Through different procedures, each of these methods eliminates the semiclassical prefactor (whose evaluation scales as the third power of the number of degrees of freedom) and the semiclassical phase, and thus attains a quasiclassical form where the dynamical observable of interest is averaged with respect to an appropriate phase space density.

The present paper deals with the derivative-FBSD formulation.<sup>45,46</sup> A number of recent calculations have demonstrated the ability of this methodology to accurately describe important dynamical processes in polyatomic systems.<sup>46,49,52,53</sup> An important step in this FBSD methodology is the evaluation of the coherent state transform of an operator related to the initial density. This quantity provides the weight of the classical trajectories, and its accurate determination is essential. While semiclassical approximations to the Boltzmann operator are possible,<sup>64</sup> the most accurate and versatile tool available for this purpose is the use of the discretized path integral (PI) formulation of quantum statistical mechanics.<sup>65</sup> A PI-FBSD procedure for evaluating time correlation functions has been described in recent papers by our group.<sup>49,52</sup> The numerical difficulty that still persists in this scheme is the presence of an oscillatory factor arising from the coherent state representation of the initial density when multiple path integral “beads” are required for an accurate representation of the Boltzmann operator.<sup>38,53</sup> Even though this factor is slowly varying, its presence becomes a serious problem when applying this method to systems with hundreds of degrees of freedom. At present, the PI-FBSD methodology developed in our group is practical for systems of 10–20 atoms over a wide range of temperatures<sup>52</sup> and also for systems with hundreds of atoms at reasonably high temperatures.<sup>53</sup>

In this paper, we develop an improved approximation for the coherent state density that makes the FBSD method applicable to simple fluids with significant quantum effects. We adopt the pair-product (PP) approximation of the imaginary time propagator,<sup>66,67</sup> a technique that amounts to a superior factorization of the Boltzmann operator, and apply it to evaluate the coherent state density. Because the pair propagator is accurate over a large temperature range, its use leads to an accurate representation of the coherent state density

with a small number of path integral beads. The dramatic reduction of the number of path integral variables achieved this way greatly facilitates convergence. In addition, the use of an imaginary time step that can be chosen much larger than that allowed by primitive propagators also leads to a considerable reduction of the oscillatory character of the integrand. In many cases the PP approximation is sufficiently accurate to allow an adequate description of the coherent state density with a single bead, thus eliminating entirely the oscillatory phase. The resulting methodology becomes applicable to dynamical calculations in quantum liquids.

We illustrate the PP-FBSD methodology by studying the self-diffusion of liquid *para*-hydrogen. The diffusion constant at several thermodynamic state points (ranging from a high-temperature liquid at  $T=25$  K to a liquid near the triple point at  $T=14$  K under nearly zero external pressure) is obtained by calculating the corresponding velocity autocorrelation functions. It is well known that liquid *para*-hydrogen in this temperature range cannot be characterized by classical liquid state theory due to its low molecular mass, and a quantum mechanical treatment is essential to the understanding of its properties. The experimentally observed self-diffusion constant<sup>68</sup> at  $T=25$  K was found to be almost three times larger than the value predicted by classical molecular dynamics simulations, an effect attributed to quantum dispersion effects. Further, collective coherent excitations, which are absent in purely classical liquids, have been observed recently by neutron scattering experiments.<sup>69,70</sup> In addition to experimental studies, extensive theoretical calculations have been also performed under these conditions. These include simulations based on centroid molecular dynamics,<sup>71–75</sup> quantum mode-coupling theory,<sup>76,77</sup> and the maximum entropy numerical analytic continuation.<sup>78</sup> The PP-FBSD results compare well with experimental measurements and other theoretical predictions.

This paper is organized as follows: In Sec. II we review briefly the FBSD method at finite temperature in conjunction with the imaginary time path integral representation of the Boltzmann operator. Then we introduce the pair-product approximation for the coherent state density and discuss its implementation in the FBSD expression for the correlation function. In Sec. III we describe the computational details for the calculation of time correlation functions of liquid *para*-hydrogen and present the results of the PP-FBSD calculations. Comparisons with experiments and other theoretical calculations are also presented in this section. Section IV contains the conclusions of this work.

## II. METHODOLOGY

In this section we review the FBSD methodology in conjunction with an imaginary time path integral evaluation of the Boltzmann operator in a coherent state representation and derive the pair-product form. Our focus is on time correlation functions at finite temperature,<sup>79</sup> which generally assume the form

$$C_{AB}(t) = \frac{1}{Z} \text{Tr}(e^{-\beta\hat{H}} \hat{A} e^{i\hat{H}t/\hbar} \hat{B} e^{-i\hat{H}t/\hbar}). \quad (2.1)$$

Here  $\hat{H}$  is the Hamiltonian of the system,  $\hat{A}$  and  $\hat{B}$  are arbitrary operators,  $\beta = 1/k_B T$  is the reciprocal temperature, and  $Z = \text{Tr}(e^{-\beta\hat{H}})$  is the canonical partition function. The three-dimensional Cartesian position and momentum vectors for the  $j$ th atom are denoted  $\mathbf{r}^{(j)}$  and  $\mathbf{p}^{(j)}$ , while the coordinates and momenta of all the particles are collected in the  $3n$ -dimensional vectors  $\mathbf{Q}$  and  $\mathbf{P}$ , respectively. The Hamiltonian for a system of  $n$  particles (atoms or rigid molecules) is written as

$$\hat{H} = \hat{H}_0 + V(\mathbf{Q}), \quad (2.2)$$

where  $\hat{H}_0$  is the operator for the total kinetic energy of the system.

$$\hat{H}_0 = \sum_{j=1}^n \hat{H}_0^{(j)}, \quad \hat{H}_0^{(j)} = \frac{|\hat{\mathbf{p}}^{(j)}|^2}{2m_j}. \quad (2.3)$$

We also define the correlation function for the inner product of two vector operators  $\hat{\mathbf{A}}$  and  $\hat{\mathbf{B}}$ :

$$C_{\mathbf{A}\cdot\mathbf{B}}(t) = \frac{1}{Z} \text{Tr}(e^{-\beta\hat{H}} \hat{\mathbf{A}} e^{i\hat{H}t/\hbar} \cdot \hat{\mathbf{B}} e^{-i\hat{H}t/\hbar}). \quad (2.4)$$

The present work aims at obtaining an accurate approximation for the coherent state representation of the Boltzmann operator entering the derivative-FBSD expression for a time correlation function obtained by Shao and Makri.<sup>45,46</sup> We note, however, the coherent state pair propagator that we develop is not linked specifically to the derivative-FBSD formulation and can also be used in conjunction with any other semiclassical representation of a time correlation function in a coherent state basis.

### A. Forward-backward semiclassical dynamics

The key idea in the FBSD formulation is to combine the forward and backward time evolution operators into a single propagator, which is then evaluated using the semiclassical approximation of time-dependent quantum mechanics in a coherent state representation. Unlike the case of influence functionals, the FBSD representation of Eq. (2.1) is not unique. The FBSD formulation of Shao and Makri,<sup>45,46</sup> which uses the derivative identity for the operator  $\hat{B}$  in conjunction with the coherent state representation of the semiclassical propagator developed by Herman and Kluk,<sup>16</sup> offers a rigorous approximation of the correlation function in the limit of  $\hbar \rightarrow 0$  that is also practical for application to systems with hundreds of atoms. Below we summarize the derivation of the derivative form of the FBSD approximation.

In the derivative FBSD formulation the Heisenberg operator entering the correlation function is written as

$$\hat{B}_H(t) = e^{i\hat{H}t/\hbar} \hat{B} e^{-i\hat{H}t/\hbar} = -i \frac{\partial}{\partial \mu} e^{i\hat{H}t/\hbar} e^{i\mu\hat{B}} e^{-i\hat{H}t/\hbar} \Big|_{\mu=0}. \quad (2.5)$$

By combining all three exponential operators into a single time evolution for an appropriate Hamiltonian along a forward-backward time contour and applying the semiclassi-

cal propagator in the coherent state representation, the Heisenberg operator can be brought into the following prefactor-free form:<sup>45,46</sup>

$$\hat{B}_H(t) = -i \frac{1}{(2\pi\hbar)^{3n}} \frac{\partial}{\partial \mu} \int d\mathbf{Q}_0 \int d\mathbf{P}_0 \exp\left(\frac{i}{\hbar} S(\mathbf{Q}_0, \mathbf{P}_0)\right) \times |G(\mathbf{Q}_f, \mathbf{P}_f)\rangle \langle G(\mathbf{Q}_0, \mathbf{P}_0)| \Big|_{\mu=0}. \quad (2.6)$$

Here  $\mathbf{Q}_0$  and  $\mathbf{P}_0$  are the initial phase space variables for classical trajectories that evolve according to the classical equations of motion corresponding to the product of three exponential operators and  $\mathbf{Q}_f$ ,  $\mathbf{P}_f$  are the phase space variables at the end of the forward-backward evolution. At the end of the forward propagation trajectories experience position and momentum jumps<sup>20</sup> (originating from the exponential of the operator  $\hat{B}$ ) according to the relation

$$\delta\mathbf{Q}_t = -\frac{1}{2} \hbar \mu \frac{\partial}{\partial \mathbf{P}_t} B(\mathbf{Q}_t, \mathbf{P}_t), \quad (2.7)$$

$$\delta\mathbf{P}_t = \frac{1}{2} \hbar \mu \frac{\partial}{\partial \mathbf{Q}_t} B(\mathbf{Q}_t, \mathbf{P}_t).$$

Here  $B(\mathbf{Q}, \mathbf{P})$  is the classical analogue of the operator  $\hat{B}$ . It is important to note<sup>45</sup> that the position and momentum jumps in Eq. (2.7) are equal to *one-half* of the values dictated by the classical equations of motion, while the action is incremented by the full amount

$$\delta S_t = \hbar \mu B(\mathbf{Q}_t, \mathbf{P}_t) + \mathbf{P}_t \cdot \delta\mathbf{Q}_t. \quad (2.8)$$

It has been shown<sup>45,46</sup> that this rescaling of the position and momentum jumps compensates for the contribution of the semiclassical prefactor. The elimination of the prefactor implies that evaluation of the full stability matrix is avoided, leading to a scheme that scales linearly with the number of degrees of freedom.<sup>46</sup>

The ket in Eq. (2.6) represents a  $3n$ -dimensional coherent state,<sup>80</sup> i.e., a product of  $n$  three-dimensional coherent states for each particle, and is described in the coordinate representation by the wave function

$$\begin{aligned} \langle \mathbf{Q} | G(\mathbf{Q}_0, \mathbf{P}_0) \rangle &= \prod_{j=1}^n \langle \mathbf{r}^{(j)} | g(\mathbf{r}_0^{(j)}, \mathbf{p}_0^{(j)}) \rangle \\ &= \left(\frac{2}{\pi}\right)^{3n/4} (\det \Gamma)^{1/4} \exp\left[-(\mathbf{Q} - \mathbf{Q}_0) \cdot \Gamma \cdot (\mathbf{Q} - \mathbf{Q}_0) + \frac{i}{\hbar} \mathbf{P}_0 \cdot (\mathbf{Q} - \mathbf{Q}_0)\right], \end{aligned} \quad (2.9)$$

where  $\Gamma$  is generally a  $3n \times 3n$  matrix. Throughout the rest of the paper we express this matrix as a diagonal matrix with elements  $\gamma_i$  representing the width parameter of the coherent state for the  $i$ th particle.

In the  $\mu \rightarrow 0$  limit the difference between forward and backward trajectories is infinitesimal. This means that interference between distinct forward and backward trajectories is neglected. Because of this, the derivative version of FBSD cannot account for long-time quantum interference effects such as wave packet rephasing.<sup>45</sup> Such long-time quantum interference is, however, often suppressed in systems with many degrees of freedom, and thus the FBSD method can provide a very accurate description of quantum dynamics in condensed phases.

The above remarks can also be used to arrive at a derivative-free form with a quasiclassical appearance. After performing some algebra, the Heisenberg operator is brought into the form<sup>51,57</sup>

$$\begin{aligned} \hat{B}_H(t) = & \frac{1}{(2\pi\hbar)^{3n}} \int d\mathbf{Q}_0 \int d\mathbf{P}_0 B(\mathbf{Q}_t, \mathbf{P}_t) \\ & \times [(1 + \frac{3}{2}n) |G(\mathbf{Q}_0, \mathbf{P}_0)\rangle \langle G(\mathbf{Q}_0, \mathbf{P}_0)| \\ & - 2\mathbf{\Gamma} \cdot (\hat{\mathbf{Q}} - \mathbf{Q}_0) |G(\mathbf{Q}_0, \mathbf{P}_0)\rangle \langle G(\mathbf{Q}_0, \mathbf{P}_0)| (\hat{\mathbf{Q}} - \mathbf{Q}_0)]. \end{aligned} \quad (2.10)$$

Here dynamical information enters exclusively via the classical function  $B$  at the phase space point reached by a trajectory at the time  $t$  of interest. Using Eq. (2.10) the correlation function for scalar operators becomes

$$\begin{aligned} C_{AB}(t) = & (2\pi\hbar)^{-3n} Z^{-1} \int d\mathbf{Q}_0 \int d\mathbf{P}_0 B(\mathbf{Q}_t, \mathbf{P}_t) \\ & \times [(1 + \frac{3}{2}n) \langle G(\mathbf{Q}_0, \mathbf{P}_0) | e^{-\beta\hat{H}} \hat{A} | G(\mathbf{Q}_0, \mathbf{P}_0) \rangle \\ & - 2 \langle G(\mathbf{Q}_0, \mathbf{P}_0) | (\hat{\mathbf{Q}} - \mathbf{Q}_0) \cdot e^{-\beta\hat{H}} \hat{A} \mathbf{\Gamma} \\ & \cdot (\hat{\mathbf{Q}} - \mathbf{Q}_0) | G(\mathbf{Q}_0, \mathbf{P}_0) \rangle], \end{aligned} \quad (2.11)$$

while the correlation function for the inner product of two vector operators takes the form

$$\begin{aligned} C_{\mathbf{A}\cdot\mathbf{B}}(t) = & (2\pi\hbar)^{-3n} Z^{-1} \int d\mathbf{Q}_0 \int d\mathbf{P}_0 (1 + \frac{3}{2}n) \\ & \times \langle G(\mathbf{Q}_0, \mathbf{P}_0) | e^{-\beta\hat{H}} \hat{\mathbf{A}} | G(\mathbf{Q}_0, \mathbf{P}_0) \rangle \cdot \mathbf{B}(\mathbf{Q}_t, \mathbf{P}_t) \\ & - 2(2\pi\hbar)^{-3n} Z^{-1} \int d\mathbf{Q}_0 \int d\mathbf{P}_0 \\ & \times \langle G(\mathbf{Q}_0, \mathbf{P}_0) | (\hat{\mathbf{Q}} - \mathbf{Q}_0) e^{-\beta\hat{H}} [\hat{\mathbf{A}} \cdot \mathbf{B}(\mathbf{Q}_t, \mathbf{P}_t)] \cdot \mathbf{\Gamma} \\ & \cdot (\hat{\mathbf{Q}} - \mathbf{Q}_0) | G(\mathbf{Q}_0, \mathbf{P}_0) \rangle. \end{aligned} \quad (2.12)$$

According to these expressions, one must propagate classical trajectories selected from a distribution obtained from the coherent state transform of an operator related to the initial density. We use this form throughout the rest of this paper.

### B. Trotter-discretized path integral representation of the coherent state density

The next step to consider is the evaluation of the coherent state (Husimi) transform of the operators appearing in Eq. (2.11), both of which involve the Boltzmann operator. A fully quantum treatment of this time-independent part is es-

sential to capture the effects of zero-point energy and reproduce the imaginary part of a correlation function. An accurate evaluation of these matrix elements is possible by using imaginary-time path integral techniques for the Boltzmann operator.<sup>65</sup> This procedure was developed recently in our group<sup>49,52</sup> and we describe it briefly here, as it relates to the approximation explored in the present study. A similar imaginary time path integral representation of coherent state matrix elements has been described by Yamamoto *et al.*<sup>40</sup>

The starting point is expression of the Boltzmann operator  $e^{-\beta\hat{H}}$  as a product of  $N$  exponential operators with imaginary time steps of length  $\Delta\beta = \beta/N$

$$e^{-\beta\hat{H}} = (e^{-\Delta\beta\hat{H}})^N. \quad (2.13)$$

By implementing the Trotter factorization<sup>81</sup> of the exponential operator  $e^{-\Delta\beta\hat{H}}$  for sufficiently small  $\Delta\beta$ ,

$$e^{-\Delta\beta\hat{H}} \simeq e^{-\Delta\beta\hat{H}_0/2} e^{-\Delta\beta\hat{V}} e^{-\Delta\beta\hat{H}_0/2}, \quad (2.14)$$

and using the closure relation, one arrives at the following expression for the first coherent state term in Eq. (2.11):

$$\begin{aligned} & \langle G(\mathbf{Q}_0, \mathbf{P}_0) | e^{-\beta\hat{H}} \hat{A} | G(\mathbf{Q}_0, \mathbf{P}_0) \rangle \\ & = \int d\mathbf{Q}_0 \int d\mathbf{P}_0 \int d\mathbf{Q}_1 \int d\mathbf{Q}_2 \cdots \\ & \times \int d\mathbf{Q}_N \langle G(\mathbf{Q}_0, \mathbf{P}_0) | e^{-\Delta\beta\hat{H}_0/2} | \mathbf{Q}_1 \rangle \\ & \times e^{-\Delta\beta V(\mathbf{Q}_1)} \langle \mathbf{Q}_1 | e^{-\Delta\beta\hat{H}_0} | \mathbf{Q}_2 \rangle \cdots e^{-\Delta\beta V(\mathbf{Q}_N)} \\ & \times \langle \mathbf{Q}_N | e^{-\Delta\beta\hat{H}_0/2} \hat{A} | G(\mathbf{Q}_0, \mathbf{P}_0) \rangle. \end{aligned} \quad (2.15)$$

Below we refer to Eq. (2.15) as the Trotter-discretized path integral representation of the coherent state transform of the Boltzmann operator. The path integral variables  $\mathbf{Q}_k$  can be thought of as fictitious classical particles that collectively describe the given delocalized quantum particle.<sup>82</sup> In the conventional PI representation of a partition function these fictitious particles form the ‘‘beads’’ of a closed necklace.<sup>82</sup> In the present coherent state representation the ends of the necklace are attached to the coherent state centers  $\mathbf{Q}_0$ , which define the initial position of a classical trajectory.<sup>49,52,53</sup> The coordinate representation of the kinetic energy part operator in Eq. (2.15) has the form

$$\begin{aligned} \langle \mathbf{Q}_k | e^{-\Delta\beta\hat{H}_0} | \mathbf{Q}_{k+1} \rangle = & \prod_{j=1}^n \left( \frac{m_j}{2\pi\hbar^2\Delta\beta} \right)^{3/2} \\ & \times \exp \left[ -\frac{m_j}{2\hbar^2\Delta\beta} |\mathbf{r}_k^{(j)} - \mathbf{r}_{k+1}^{(j)}|^2 \right], \end{aligned} \quad (2.16)$$

and the first coherent state matrix element is given analytically by the expression

$$\begin{aligned} & \langle \mathbf{Q} | e^{-\Delta\beta\hat{H}_0/2} | G(\mathbf{Q}_0, \mathbf{P}_0) \rangle \\ &= \prod_{j=1}^n \left( \frac{2\gamma_j}{\pi} \right)^{3/4} \left( \frac{m_j}{m_j + \hbar^2 \Delta\beta \gamma_j} \right)^{3/2} \\ & \times \exp \left\{ -\frac{m_j}{m_j + \hbar^2 \Delta\beta \gamma_j} \left[ \gamma_j |\mathbf{r}^{(j)} - \mathbf{r}_0^{(j)}|^2 \right. \right. \\ & \left. \left. + \frac{\Delta\beta}{4m} |\mathbf{p}_0^{(j)}|^2 - \frac{i}{\hbar} \mathbf{p}_0^{(j)} \cdot (\mathbf{r}^{(j)} - \mathbf{r}_0^{(j)}) \right] \right\}. \end{aligned} \quad (2.17)$$

The other coherent state matrix element depends on the form of operator  $\hat{A}$ . If  $\hat{A}$  is given by a simple polynomial, this matrix element can be expressed in a form

$$\begin{aligned} & \langle \mathbf{Q} | e^{-\Delta\beta\hat{H}_0/2} \hat{A} | G(\mathbf{Q}_0, \mathbf{P}_0) \rangle \\ &= a(\mathbf{Q}_0, \mathbf{P}_0, \mathbf{Q}) \langle \mathbf{Q} | e^{-\Delta\beta\hat{H}_0/2} | G(\mathbf{Q}_0, \mathbf{P}_0) \rangle, \end{aligned} \quad (2.18)$$

where  $a(\mathbf{Q}_0, \mathbf{P}_0, \mathbf{Q})$  is a function that depends on the form of operator  $\hat{A}$ .

The second coherent state term in Eq. (2.11) can also be described in the discretized path integral representation as

$$\begin{aligned} & \langle G(\mathbf{Q}_0, \mathbf{P}_0) | (\hat{\mathbf{Q}} - \mathbf{Q}_0) \cdot e^{-\beta\hat{H}} \hat{A} \Gamma \cdot (\hat{\mathbf{Q}} - \mathbf{Q}_0) | G(\mathbf{Q}_0, \mathbf{P}_0) \rangle \\ &= \int d\mathbf{Q}_0 \int d\mathbf{P}_0 \int d\mathbf{Q}_1 \int d\mathbf{Q}_2 \cdots \\ & \times \int d\mathbf{Q}_N \langle G(\mathbf{Q}_0, \mathbf{P}_0) | (\hat{\mathbf{Q}} - \mathbf{Q}_0) e^{-\Delta\beta\hat{H}_0/2} | \mathbf{Q}_1 \rangle \\ & \times e^{-\Delta\beta V(\mathbf{Q}_1)} \langle \mathbf{Q}_1 | e^{-\Delta\beta\hat{H}_0} | \mathbf{Q}_2 \rangle \cdots e^{-\Delta\beta V(\mathbf{Q}_N)} \\ & \times \langle \mathbf{Q}_N | e^{-\Delta\beta\hat{H}_0/2} \hat{A} \Gamma \cdot (\hat{\mathbf{Q}} - \mathbf{Q}_0) | G(\mathbf{Q}_0, \mathbf{P}_0) \rangle. \end{aligned} \quad (2.19)$$

The coherent state factors in this expression are also easily evaluated. Combining these expressions, the Trotter-discretized path integral representation of the FBSD correlation functions considered earlier takes the form

$$\begin{aligned} C_{AB}(t) &= (2\pi\hbar)^{-3n} \int d\mathbf{Q}_0 \int d\mathbf{P}_0 \int d\mathbf{Q}_1 \cdots \\ & \times \int d\mathbf{Q}_N \Theta(\mathbf{Q}_0, \mathbf{P}_0, \mathbf{Q}_1, \dots, \mathbf{Q}_N) \\ & \times \Lambda_{AB}(\mathbf{Q}_0, \mathbf{P}_0, \mathbf{Q}_1, \dots, \mathbf{Q}_N), \\ C_{A\cdot B}(t) &= (2\pi\hbar)^{-3n} \int d\mathbf{Q}_0 \int d\mathbf{P}_0 \int d\mathbf{Q}_1 \cdots \\ & \times \int d\mathbf{Q}_N \Theta(\mathbf{Q}_0, \mathbf{P}_0, \mathbf{Q}_1, \dots, \mathbf{Q}_N) \\ & \times \Lambda_{A\cdot B}(\mathbf{Q}_0, \mathbf{P}_0, \mathbf{Q}_1, \dots, \mathbf{Q}_N). \end{aligned} \quad (2.20)$$

In these equations

$$\begin{aligned} \Theta(\mathbf{Q}_0, \mathbf{P}_0, \mathbf{Q}_1, \dots, \mathbf{Q}_N) &= Z^{-1} \langle G(\mathbf{Q}_0, \mathbf{P}_0) | e^{-\Delta\beta\hat{H}_0/2} | \mathbf{Q}_1 \rangle e^{-\Delta\beta V(\mathbf{Q}_1)} \langle \mathbf{Q}_1 | e^{-\Delta\beta\hat{H}_0} | \mathbf{Q}_2 \rangle \cdots e^{-\Delta\beta V(\mathbf{Q}_N)} \langle \mathbf{Q}_N | e^{-\Delta\beta\hat{H}_0/2} | G(\mathbf{Q}_0, \mathbf{P}_0) \rangle \\ &= Z^{-1} \prod_{j=1}^n \left( \frac{2\gamma_j}{\pi} \right)^{3/2} \left( \frac{m_j}{m_j + \hbar^2 \Delta\beta \gamma_j} \right)^3 \left( \frac{m_j}{2\pi\hbar^2 \Delta\beta} \right)^{3(N-1)/2} \\ & \times \exp \left\{ -\sum_{j=1}^n \frac{m_j}{m_j + \hbar^2 \Delta\beta \gamma_j} \left( \gamma_j |\mathbf{r}_1^{(j)} - \mathbf{r}_0^{(j)}|^2 + \gamma_j |\mathbf{r}_N^{(j)} - \mathbf{r}_0^{(j)}|^2 + \frac{i}{\hbar} \mathbf{p}_0^{(j)} \cdot (\mathbf{r}_1^{(j)} - \mathbf{r}_N^{(j)}) + \frac{\Delta\beta}{2m_j} |\mathbf{p}_0^{(j)}|^2 \right) \right. \\ & \left. - \sum_{j=1}^n \frac{m_j}{2\hbar^2 \Delta\beta} \sum_{k=2}^N |\mathbf{r}_k^{(j)} - \mathbf{r}_{k-1}^{(j)}|^2 - \Delta\beta \sum_{k=1}^N V(\mathbf{Q}_k) \right\}, \end{aligned} \quad (2.21)$$

is the integrand in the Trotter-discretized path integral representation of the coherent state transform of the Boltzmann operator, and the functions  $\Lambda_{AB}$  and  $\Lambda_{A\cdot B}$  depend upon the form of the operator  $\hat{A}$ .

The multidimensional integral appearing in Eq. (2.20) is usually performed by Monte Carlo methods. We use the modulus of the entire exponential part as the sampling function:

$$\begin{aligned} & \mathcal{P}(\mathbf{Q}_0, \mathbf{P}_0, \mathbf{Q}_1, \mathbf{Q}_2, \dots, \mathbf{Q}_N) \\ &= |\langle G(\mathbf{Q}_0, \mathbf{P}_0) | e^{-\Delta\beta\hat{H}_0/2} | \mathbf{Q}_1 \rangle e^{-\Delta\beta V(\mathbf{Q}_1)} \\ & \times \langle \mathbf{Q}_1 | e^{-\Delta\beta\hat{H}_0} | \mathbf{Q}_2 \rangle \cdots e^{-\Delta\beta V(\mathbf{Q}_N)} \\ & \times \langle \mathbf{Q}_N | e^{-\Delta\beta\hat{H}_0/2} | G(\mathbf{Q}_0, \mathbf{P}_0) \rangle|. \end{aligned} \quad (2.22)$$

Since the integral of this sampling function is not necessarily proportional to the partition function, one has to perform a separate Monte Carlo calculation to obtain normalized results. These procedures are detailed in Ref. 52. A molecular dynamics sampling technique that provides efficient sampling of initial phase space and path integral variables was recently developed in our group.<sup>53</sup>

As has been seen thus far, the FBSD method sidesteps the problem associated with phase cancellation arising from the action entering the semiclassical propagator and thus makes Monte Carlo evaluation feasible. As demonstrated by several recent calculations,<sup>46,52,53</sup> this method is robust and practical for systems with at least several tens of degrees of freedom. However, the presence of a mildly oscillating factor arising from the path integral representation of the coherent state density,

$$\prod_{j=1}^n \exp\left[-\frac{i}{\hbar} \frac{m_j}{m_j + \hbar^2 \Delta \beta \gamma_j} \mathbf{p}_0^{(j)} \cdot (\mathbf{r}_1^{(j)} - \mathbf{r}_N^{(j)})\right], \quad (2.23)$$

can become an obstacle. Although this is a slowly varying factor, it can prevent convergence of Monte Carlo methods in simulations of condensed phase systems that often involve hundreds of particles, because the phase cancellation problem becomes worse at an exponential rate as the system size increases. One of the strategies to circumvent this problem may be to use sufficiently large values of  $\gamma_j$  in order to damp this oscillatory factor. Experience from simulations of simple liquids in our group indicates that Monte Carlo evaluation of the multi-bead PI-FBSD expressions presented in the previous subsection can converge only if the value of the coherent state parameter is orders of magnitude larger than that suggested from the time scales of the interaction potential. However, the FBSD approximation has been shown to degrade when the coherent state parameter exceeds significantly its optimal value.<sup>83</sup> In addition, the coherent state parameters  $\gamma_j$  determines initial momentum distributions [see Eq. (2.21)], and a large value of  $\gamma_j$  corresponds to a very wide distribution in momentum space, which in turn introduces a serious numerical problem.

The phase cancellation problem associated with the coherent state functions disappears in the single bead ( $N=1$ ) limit. This limit provides an accurate representation of the Boltzmann operator under nearly classical conditions, i.e., if the Trotter factorization with an imaginary time step  $\beta/2$  is sufficiently accurate. The single-bead high-temperature limit of the PI-FBSD methodology is appealing in itself, as it can account for nonzero imaginary components of correlation functions even within this nearly classical treatment. This feature is a consequence of the use of a coherent state representation of the density.<sup>52,53</sup>

The validity of applying the single-bead approximation depends of course on the thermal de Broglie wavelength of a particle<sup>65</sup> and becomes inadequate under conditions where quantum effects are large. It can be easily shown that the expectation value of the kinetic energy obtained from the single-bead PI-FBSD expression coincides with the result of classical mechanics. It is well known that the kinetic energy of quantum liquids exceeds the classical estimate. For example, a path integral Monte Carlo calculation for liquid

*para*-hydrogen at  $T=25$  K gives a kinetic energy equal to 62 K/particle under zero external pressure,<sup>84</sup> which differs significantly from the classical estimate of 37.5 K/particle. It is obvious that quantum effects such as zero-point energy are prevalent under these conditions and that use of only one path integral bead is not adequate in this case. Since a finer discretization of the Boltzmann operator based on multiple Trotter steps is impractical in condensed phase systems due to severe phase cancellation, we turn our attention to superior single-bead approximations.

### C. Pair-product approximation

Our aim here is to devise a good approximation for matrix elements of the type  $\langle \mathbf{Q} | \exp(-\tau \hat{H}) | G(\mathbf{Q}_0, \mathbf{P}_0) \rangle$  that allows a larger value of imaginary time step  $\tau$  compared to that required for convergence of the primitive form obtained with the Trotter factorization. If this could be made accurate enough for  $\tau = \beta/2$ , one would be able to use a single path integral bead and avoid serious phase cancellation. The problem of constructing improved propagators for use in path integral calculations has been discussed extensively. Several methods have been proposed toward this direction, including the use of exponential power series expansions,<sup>85</sup> cumulant approaches,<sup>86</sup> harmonic reference methods,<sup>87</sup> and propagators based on an adiabatic splitting of the Hamiltonian.<sup>88</sup> Our approach in the present study employs the pair-product approximation developed mainly in the context of liquid helium at low temperatures.<sup>66,67</sup> This approximation leads to the most efficient method for a system with pair-wise additive interactions, which we investigate in this work. Throughout the rest of this paper we focus on isotropic fluids.

Consider a pair of two atoms, with coordinates and momenta  $\mathbf{r}^{(1)}$ ,  $\mathbf{p}^{(1)}$  and  $\mathbf{r}^{(2)}$ ,  $\mathbf{p}^{(2)}$ , respectively. Defining center-of-mass and relative coordinates

$$\mathbf{R}^{(12)} = \frac{1}{2}(\mathbf{r}^{(1)} + \mathbf{r}^{(2)}) \quad \text{and} \quad \mathbf{r}^{(12)} = \mathbf{r}^{(1)} - \mathbf{r}^{(2)}, \quad (2.24)$$

and performing a canonical transformation, the Hamiltonian for this pair of atoms

$$H^{(12)} = \frac{|\mathbf{p}^{(1)}|^2 + |\mathbf{p}^{(2)}|^2}{2m} + V^{(12)}(|\mathbf{r}^{(1)} - \mathbf{r}^{(2)}|), \quad (2.25)$$

is rewritten in the form

$$H^{(12)} = H_{\text{trans}}^{(12)} + H_{\text{int}}^{(12)}, \quad (2.26)$$

where

$$H_{\text{trans}}^{(12)} = \frac{|\mathbf{P}^{(12)}|^2}{2M},$$

$$H_{\text{int}}^{(12)} = \frac{|\mathbf{p}^{(12)}|^2}{2\mu} + V^{(12)}(|\mathbf{r}^{(12)}|) \equiv T_{\text{int}}^{(12)} + V^{(12)}(|\mathbf{r}^{(12)}|), \quad (2.27)$$

are the Hamiltonians describing the center-of-mass (translational) and relative (internal) motion, respectively. In Eq. (2.27)  $\mathbf{P}^{(12)}$ ,  $\mathbf{p}^{(12)}$  are momenta conjugate to the coordinates  $\mathbf{R}^{(12)}$ ,  $\mathbf{r}^{(12)}$ , respectively, and  $M = 2m$ ,  $\mu = m/2$ . Using Eq. (2.26) the coordinate matrix element of the Boltzmann operator for an arbitrary imaginary time step  $\tau$  is factored into a

free-particle part corresponding to the motion of the center of mass and the matrix element of the Hamiltonian describing internal motion:

$$\begin{aligned} & \langle \mathbf{r}_k^{(1)} \mathbf{r}_k^{(2)} | \exp(-\tau \hat{H}^{(12)}) | \mathbf{r}_{k'}^{(1)} \mathbf{r}_{k'}^{(2)} \rangle \\ &= \langle \mathbf{R}_k^{(12)} | \exp(-\tau \hat{H}_{\text{trans}}^{(12)}) | \mathbf{R}_{k'}^{(12)} \rangle \\ & \quad \times \langle \mathbf{r}_k^{(12)} | \exp(-\tau \hat{H}_{\text{int}}^{(12)}) | \mathbf{r}_{k'}^{(12)} \rangle. \end{aligned} \quad (2.28)$$

Application of the same transformation to the Boltzmann operator for the total kinetic energy  $\hat{H}_0^{(12)} = (|\hat{\mathbf{p}}^{(1)}|^2 + |\hat{\mathbf{p}}^{(2)}|^2)/2m$  for the same two-atom system gives the result

$$\begin{aligned} & \langle \mathbf{r}_k^{(1)} \mathbf{r}_k^{(2)} | \exp(-\tau \hat{H}_0^{(12)}) | \mathbf{r}_{k'}^{(1)} \mathbf{r}_{k'}^{(2)} \rangle \\ &= \langle \mathbf{R}_k^{(12)} | \exp(-\tau \hat{H}_{\text{trans}}^{(12)}) | \mathbf{R}_{k'}^{(12)} \rangle \\ & \quad \times \langle \mathbf{r}_k^{(12)} | \exp(-\tau \hat{T}_{\text{int}}^{(12)}) | \mathbf{r}_{k'}^{(12)} \rangle. \end{aligned} \quad (2.29)$$

Use of Eqs. (2.28) and (2.29) leads to the result

$$\begin{aligned} & \langle \mathbf{r}_k^{(1)} \mathbf{r}_k^{(2)} | \exp(-\tau \hat{H}^{(12)}) | \mathbf{r}_{k'}^{(1)} \mathbf{r}_{k'}^{(2)} \rangle \\ &= \langle \mathbf{r}_k^{(1)} | \exp(-\tau \hat{H}_0^{(1)}) | \mathbf{r}_{k'}^{(1)} \rangle \langle \mathbf{r}_k^{(2)} | \exp(-\tau \hat{H}_0^{(2)}) | \mathbf{r}_{k'}^{(2)} \rangle \\ & \quad \times \exp(-\varphi(\mathbf{r}_k^{(12)}, \mathbf{r}_{k'}^{(12)})), \end{aligned} \quad (2.30)$$

where

$$\exp(-\varphi(\mathbf{r}_k^{(12)}, \mathbf{r}_{k'}^{(12)})) = \frac{\langle \mathbf{r}_k^{(12)} | \exp(-\tau \hat{H}_{\text{int}}^{(12)}) | \mathbf{r}_{k'}^{(12)} \rangle}{\langle \mathbf{r}_k^{(12)} | \exp(-\tau \hat{T}_{\text{int}}^{(12)}) | \mathbf{r}_{k'}^{(12)} \rangle}. \quad (2.31)$$

The first two factors in Eq. (2.30) are matrix elements of the Boltzmann operator for two noninteracting particles. Potential interactions are taken into account *exactly* through the function  $\varphi$ .

Consider now the coherent state function for a single particle

$$\begin{aligned} \langle \mathbf{r}_k^{(1)} | g_{\gamma}(\mathbf{r}_0^{(1)}, \mathbf{p}_0^{(1)}) \rangle &= \left( \frac{2\gamma}{\pi} \right)^{3/4} \exp\left( -\gamma |\mathbf{r}_k^{(1)} - \mathbf{r}_0^{(1)}|^2 \right. \\ & \quad \left. + \frac{i}{\hbar} \mathbf{p}_0^{(1)} \cdot (\mathbf{r}_k^{(1)} - \mathbf{r}_0^{(1)}) \right). \end{aligned} \quad (2.32)$$

It is easy to show that the coherent state for the two-particle pair can be brought into the form

$$\begin{aligned} & \langle \mathbf{r}_k^{(1)} | g_{\gamma}(\mathbf{r}_0^{(1)}, \mathbf{p}_0^{(1)}) \rangle \langle \mathbf{r}_k^{(2)} | g_{\gamma}(\mathbf{r}_0^{(2)}, \mathbf{p}_0^{(2)}) \rangle \\ &= \langle \mathbf{R}_k^{(12)} | g_{2\gamma}(\mathbf{R}_0^{(12)}, 2\mathbf{P}_0^{(12)}) \rangle \langle \mathbf{r}_k^{(12)} | g_{\gamma/2}(\mathbf{r}_0^{(12)}, \frac{1}{2}\mathbf{p}_0^{(12)}) \rangle. \end{aligned} \quad (2.33)$$

The first factor in the right-hand-side of Eq. (2.33) is a coherent state for the translational motion of the pair, while the second one describes internal motion. Inserting a complete set of position states for each atom and making use of the pair propagator relation in the coordinate representation, Eq. (2.30), the matrix element for the two-particle system becomes

$$\begin{aligned} & \langle \mathbf{r}_k^{(1)} \mathbf{r}_k^{(2)} | \exp(-\tau \hat{H}^{(12)}) | g_{\gamma}(\mathbf{r}_0^{(1)}, \mathbf{p}_0^{(1)}) g_{\gamma}(\mathbf{r}_0^{(2)}, \mathbf{p}_0^{(2)}) \rangle \\ &= \int d\tilde{\mathbf{r}}^{(1)} \int d\tilde{\mathbf{r}}^{(2)} \langle \mathbf{r}_k^{(1)} | \exp(-\tau \hat{H}_0^{(1)}) | \tilde{\mathbf{r}}^{(1)} \rangle \\ & \quad \times \langle \mathbf{r}_k^{(2)} | \exp(-\tau \hat{H}_0^{(2)}) | \tilde{\mathbf{r}}^{(2)} \rangle \exp(-\varphi(\mathbf{r}_k^{(12)}, \tilde{\mathbf{r}}^{(12)})) \\ & \quad \times \langle \tilde{\mathbf{r}}^{(1)} | g_{\gamma}(\mathbf{r}_0^{(1)}, \mathbf{p}_0^{(1)}) \rangle \langle \tilde{\mathbf{r}}^{(2)} | g_{\gamma}(\mathbf{r}_0^{(2)}, \mathbf{p}_0^{(2)}) \rangle. \end{aligned} \quad (2.34)$$

A change of integration variables to center-of-mass and relative coordinates, along with Eqs. (2.29) and (2.33) brings the desired matrix element to the form

$$\begin{aligned} & \langle \mathbf{r}_k^{(1)} \mathbf{r}_k^{(2)} | \exp(-\tau \hat{H}^{(12)}) | g_{\gamma}(\mathbf{r}_0^{(1)}, \mathbf{p}_0^{(1)}) g_{\gamma}(\mathbf{r}_0^{(2)}, \mathbf{p}_0^{(2)}) \rangle \\ &= \int d\tilde{\mathbf{R}}^{(12)} \int d\tilde{\mathbf{r}}^{(12)} \langle \mathbf{R}_k^{(12)} | \exp(-\tau \hat{H}_{\text{trans}}^{(12)}) | \tilde{\mathbf{R}}^{(12)} \rangle \\ & \quad \times \langle \mathbf{r}_k^{(12)} | \exp(-\tau \hat{T}_{\text{int}}^{(12)}) | \tilde{\mathbf{r}}^{(12)} \rangle \\ & \quad \times \exp(-\varphi(\mathbf{r}_k^{(12)}, \tilde{\mathbf{r}}^{(12)})) \langle \tilde{\mathbf{R}}^{(12)} | g_{2\gamma}(\mathbf{R}_0^{(12)}, 2\mathbf{P}_0^{(12)}) \rangle \\ & \quad \times \langle \tilde{\mathbf{r}}^{(12)} | g_{\gamma/2}(\mathbf{r}_0^{(12)}, \frac{1}{2}\mathbf{p}_0^{(12)}) \rangle. \end{aligned} \quad (2.35)$$

This can be written as a product of two integrals, and use of Eq. (2.31) leads to the expression

$$\begin{aligned} & \langle \mathbf{r}_k^{(1)} \mathbf{r}_k^{(2)} | \exp(-\tau \hat{H}^{(12)}) | g_{\gamma}(\mathbf{r}_0^{(1)}, \mathbf{p}_0^{(1)}) g_{\gamma}(\mathbf{r}_0^{(2)}, \mathbf{p}_0^{(2)}) \rangle \\ &= \int d\tilde{\mathbf{R}}^{(12)} \langle \mathbf{R}_k^{(12)} | \exp(-\tau \hat{H}_{\text{trans}}^{(12)}) | \tilde{\mathbf{R}}^{(12)} \rangle \\ & \quad \times \langle \tilde{\mathbf{R}}^{(12)} | g_{2\gamma}(\mathbf{R}_0^{(12)}, 2\mathbf{P}_0^{(12)}) \rangle \\ & \quad \times \int d\tilde{\mathbf{r}}^{(12)} \langle \mathbf{r}_k^{(12)} | \exp(-\tau \hat{H}_{\text{int}}^{(12)}) | \tilde{\mathbf{r}}^{(12)} \rangle \\ & \quad \times \langle \tilde{\mathbf{r}}^{(12)} | g_{\gamma/2}(\mathbf{r}_0^{(12)}, \frac{1}{2}\mathbf{p}_0^{(12)}) \rangle. \end{aligned} \quad (2.36)$$

It is easy to show that the first integral in the last equation can be written as

$$\begin{aligned} & \langle \mathbf{R}_k^{(12)} | \exp(-\tau \hat{H}_{\text{trans}}^{(12)}) | g_{2\gamma}(\mathbf{R}_0^{(12)}, 2\mathbf{P}_0^{(12)}) \rangle \\ &= \langle \mathbf{r}_k^{(1)} | \exp(-\tau \hat{H}_0^{(1)}) | g_{\gamma}(\mathbf{r}_0^{(1)}, \mathbf{p}_0^{(1)}) \rangle \\ & \quad \times \langle \mathbf{r}_k^{(2)} | \exp(-\tau \hat{H}_0^{(2)}) | g_{\gamma}(\mathbf{r}_0^{(2)}, \mathbf{p}_0^{(2)}) \rangle \\ & \quad \times \langle \mathbf{r}_k^{(12)} | \exp(-\tau \hat{T}_{\text{int}}^{(12)}) | g_{\gamma/2}(\mathbf{r}_0^{(12)}, \frac{1}{2}\mathbf{p}_0^{(12)}) \rangle^{-1}. \end{aligned} \quad (2.37)$$

Using this expression, the desired matrix element is written in the final form

$$\begin{aligned} & \langle \mathbf{r}_k^{(1)} \mathbf{r}_k^{(2)} | \exp(-\tau \hat{H}^{(12)}) | g_{\gamma}(\mathbf{r}_0^{(1)}, \mathbf{p}_0^{(1)}) g_{\gamma}(\mathbf{r}_0^{(2)}, \mathbf{p}_0^{(2)}) \rangle \\ &= \langle \mathbf{r}_k^{(1)} | \exp(-\tau \hat{H}_0^{(1)}) | g_{\gamma}(\mathbf{r}_0^{(1)}, \mathbf{p}_0^{(1)}) \rangle \\ & \quad \times \langle \mathbf{r}_k^{(2)} | \exp(-\tau \hat{H}_0^{(2)}) | g_{\gamma}(\mathbf{r}_0^{(2)}, \mathbf{p}_0^{(2)}) \rangle \\ & \quad \times \exp(-u(\mathbf{r}_k^{(12)}, \mathbf{r}_0^{(12)}, \mathbf{p}_0^{(12)})), \end{aligned} \quad (2.38)$$

where

$$\exp(-u(\mathbf{r}_k^{(12)}, \mathbf{r}_0^{(12)}, \mathbf{p}_0^{(12)})) = \frac{\int d\tilde{\mathbf{r}}^{(12)} \langle \mathbf{r}_k^{(12)} | \exp(-\tau \hat{H}_{\text{int}}^{(12)}) | \tilde{\mathbf{r}}^{(12)} \rangle \langle \tilde{\mathbf{r}}^{(12)} | g_{\gamma/2}(\mathbf{r}_0^{(12)}, \frac{1}{2} \mathbf{p}_0^{(12)}) \rangle}{\langle \mathbf{r}_k^{(12)} | \exp(-\tau \hat{T}_{\text{int}}^{(12)}) | g_{\gamma/2}(\mathbf{r}_0^{(12)}, \frac{1}{2} \mathbf{p}_0^{(12)}) \rangle}. \quad (2.39)$$

The mixed coordinate-coherent state matrix elements of the free particle Boltzmann operator that appear in the Eqs. (2.38) and (2.39) are given by the expression

$$\begin{aligned} & \langle \mathbf{r}_k^{(1)} | \exp(-\tau \hat{H}_0^{(1)}) | g_\gamma(\mathbf{r}_0^{(1)}, \mathbf{p}_0^{(1)}) \rangle \\ &= \left( \frac{2\gamma}{\pi} \right)^{3/4} \left( \frac{m}{m + 2\hbar^2 \tau \gamma} \right)^{3/2} \exp \left[ -\frac{m}{m + 2\hbar^2 \tau \gamma} \right. \\ & \quad \times \left\{ \gamma |\mathbf{r}_k^{(1)} - \mathbf{r}_0^{(1)}|^2 + \frac{\tau}{2m} |\mathbf{p}_0^{(1)}|^2 - \frac{i}{\hbar} \mathbf{p}_0^{(1)} \cdot (\mathbf{r}_k^{(1)} \right. \\ & \quad \left. \left. - \mathbf{r}_0^{(1)}) \right\} \right]. \quad (2.40) \end{aligned}$$

By definition, the pair propagator given by Eqs. (2.38) and (2.40) is exact for a pair of particles.

By employing this interaction term  $u(\mathbf{r}, \mathbf{r}_0, \mathbf{p}_0)$  for a pair of particles, we approximate the matrix element of the Boltzmann operator for the total Hamiltonian as

$$\begin{aligned} & \langle \mathbf{Q} | \exp(-\tau \hat{H}) | G(\mathbf{Q}_0, \mathbf{P}_0) \rangle \\ & \simeq \prod_{i=1}^n \langle \mathbf{r}^{(i)} | \exp(-\tau \hat{H}_0^{(i)}) | g_\gamma(\mathbf{r}_0^{(i)}, \mathbf{p}_0^{(i)}) \rangle \\ & \quad \times \prod_{i < j}^n \exp(-u(\mathbf{r}^{(ij)}, \mathbf{r}_0^{(ij)}, \mathbf{p}_0^{(ij)})). \quad (2.41) \end{aligned}$$

This interaction term can be seen as an effective potential. In the high temperature limit  $u(\mathbf{r}, \mathbf{r}_0, \mathbf{p}_0)$  approaches  $\tau V(\mathbf{r})$  and thus the PP reduces to the standard Trotter product.<sup>81</sup> However, as will be seen later, this method captures nontrivial quantum effects such as zero-point energy in a satisfactory manner even if only a single path integral bead is used. It is worth noting that this effective potential  $u(\mathbf{r}, \mathbf{r}_0, \mathbf{p}_0)$  is complex valued, but the magnitude of the imaginary part of  $\exp(-u(\mathbf{r}, \mathbf{r}_0, \mathbf{p}_0))$  is normally very small compared to that of the real part. The oscillatory feature of the above matrix element comes mainly from the matrix element of the free-particle part.

The intra-pair density matrix element  $\langle \mathbf{r}^{(12)} | \exp(-\tau \hat{H}_{\text{int}}^{(12)}) | \tilde{\mathbf{r}}^{(12)} \rangle$  appearing in Eq. (2.39) needs to be evaluated in order to obtain an effective potential  $u(\mathbf{r}^{(12)}, \mathbf{r}_0^{(12)}, \mathbf{p}_0^{(12)})$ . If the interaction potential between particles is isotropic, one can expand this three-dimensional density matrix in terms of partial waves. Each partial wave component is the one-dimensional density matrix with an additional centrifugal term, which can be evaluated efficiently by the matrix-squaring method.<sup>67</sup> These techniques to obtain the density matrix for a pair of particles are explained in detail in Ref. 67. The coordinate matrix element is evaluated once and stored in memory.

Further, in order to evaluate an effective potential  $u(\mathbf{r}^{(12)}, \mathbf{r}_0^{(12)}, \mathbf{p}_0^{(12)})$  one needs to perform a three-dimensional

integral as shown in Eq. (2.39). From a computational point of view it seems beneficial to consider fitting or constructing a table of this effective potential prior to the start of Monte Carlo sampling. Unfortunately, this term depends on six variables even if symmetry is exploited to reduce dimensionality, and one must also evaluate the first and second derivatives of this function in order to obtain relevant matrix elements (see, e.g., the next paragraph). These facts lead the conclusion that explicit construction of a table is inappropriate in this case. Additionally, fitting to some functions is not straightforward in this case. Another option is to reduce this three-dimensional integral to a one-dimensional one by transforming to spherical polar coordinates and expanding the various terms in spherical harmonics. However, the advantage gained this way is offset by the need to sum over terms whose expansion coefficients are related to vector-coupling coefficients. At large values of  $\mathbf{p}_0^{(12)}$  many terms are necessary to achieve convergence.

After some investigations, we conclude that direct evaluation of this three-dimensional integral during the Monte Carlo procedure is both accurate and efficient. Because the integrand of Eq. (2.39) contains a Gaussian factor, it is efficiently evaluated using a Gauss-Hermite quadrature. For this task we define a Cartesian coordinate system  $(\tilde{x}, \tilde{y}, \tilde{z})$  with origin at  $(m\mathbf{r}^{(12)} + 2\hbar^2 \tau \gamma \mathbf{r}_0^{(12)}) / (m + 2\hbar^2 \tau \gamma)$  with the  $\tilde{z}$  axis pointing along  $\mathbf{p}_0^{(12)}$ . With this choice the integrand has a constant phase at a fixed value of  $\tilde{z}$  and thus is a smooth function of  $\tilde{x}$  and  $\tilde{y}$ , allowing integration with a small number of quadrature points along these coordinates. Evaluation of the derivatives of  $u(\mathbf{r}^{(12)}, \mathbf{r}_0^{(12)}, \mathbf{p}_0^{(12)})$  is performed by differentiating Eq. (2.39) and evaluating the resulting integrals in a similar manner. While primitive, this procedure is accurate and the entire FBSD calculation can be done within moderate CPU time.

As has been shown in several applications<sup>66,67</sup> (and will also be demonstrated through the numerical calculations presented in the next section), the use of the pair-product approximation allows accurate determination of the imaginary time propagator with time steps that are between one and two orders of magnitude larger than those necessary in the primitive Trotter approximation. Thus, the use of the pair-product approximation in the discretized path integral form of the FBSD correlation function should dramatically reduce the required number of beads, facilitating calculations in systems with several tens of particles at very low temperatures. Further, because the high accuracy of the PP approximation allows the use of a larger imaginary time step, the oscillatory character of Eq. (2.40) is reduced significantly compared to the Trotter expression. In the present paper, however, we develop the PP-FBSD formulation of time correlation functions in the most practical single bead limit and demonstrate its ability to model fluids at low temperature where quantum effects are dominant.

Below we use Eq. (2.41) to obtain a single-bead PP-FBSD expression for the momentum correlation function for an isotropic fluid. Inserting a complete set of coordinate states in Eq. (2.12), the correlation function for the total momentum vector becomes

$$\begin{aligned}
 C_{\mathbf{P},\mathbf{P}}(t) &= (2\pi\hbar)^{-3n} Z^{-1} \int d\mathbf{Q}_0 \int d\mathbf{P}_0 \int d\mathbf{Q}_1 \\
 &\times [(1 + \frac{3}{2}n) \langle G(\mathbf{Q}_0, \mathbf{P}_0) | e^{-\beta\hat{H}/2} | \mathbf{Q}_1 \rangle \\
 &\times \langle \mathbf{Q}_1 | e^{-\beta\hat{H}/2} \hat{\mathbf{P}} | G(\mathbf{Q}_0, \mathbf{P}_0) \rangle \cdot \mathbf{P}_t \\
 &- 2 \langle G(\mathbf{Q}_0, \mathbf{P}_0) | (\hat{\mathbf{Q}} - \mathbf{Q}_0) e^{-\beta\hat{H}/2} | \mathbf{Q}_1 \rangle \langle \mathbf{Q}_1 | e^{-\beta\hat{H}/2} \\
 &\times (\hat{\mathbf{P}} \cdot \mathbf{P}_t) \Gamma \cdot (\hat{\mathbf{Q}} - \mathbf{Q}_0) | G(\mathbf{Q}_0, \mathbf{P}_0) \rangle]. \quad (2.42)
 \end{aligned}$$

The various matrix elements in this expression can be written in terms of matrix elements of the Boltzmann operator alone. For example,

$$\begin{aligned}
 \langle \mathbf{Q}_1 | e^{-\beta\hat{H}/2} \hat{\mathbf{P}} | G(\mathbf{Q}_0, \mathbf{P}_0) \rangle \\
 = i\hbar \frac{\partial}{\partial \mathbf{Q}_0} \langle \mathbf{Q}_1 | e^{-\beta\hat{H}/2} | G(\mathbf{Q}_0, \mathbf{P}_0) \rangle. \quad (2.43)
 \end{aligned}$$

After some algebra, the PP-FBSD expression for the momentum autocorrelation function becomes

$$\begin{aligned}
 C_{\mathbf{P},\mathbf{P}}(t) &= (2\pi\hbar)^{-3n} \int d\mathbf{Q}_0 \int d\mathbf{P}_0 \\
 &\times \int d\mathbf{Q}_1 \tilde{\Theta}(\mathbf{Q}_0, \mathbf{P}_0, \mathbf{Q}_1) \tilde{\Lambda}_{\mathbf{P},\mathbf{P}}(\mathbf{Q}_0, \mathbf{P}_0, \mathbf{Q}_1). \quad (2.44)
 \end{aligned}$$

The function  $\tilde{\Theta}$  is the pair-product analogue of Eq. (2.21), which depends on the effective potential  $u$ , and  $\tilde{\Lambda}_{\mathbf{P},\mathbf{P}}$  is a nonexponential factor that contains the first two derivatives of  $u$ . The Monte Carlo sampling function is chosen as the absolute value of the exponential factor,

$$\begin{aligned}
 \mathcal{P}(\mathbf{Q}_0, \mathbf{P}_0, \mathbf{Q}_1) &= |\tilde{\Theta}(\mathbf{Q}_0, \mathbf{P}_0, \mathbf{Q}_1)| \\
 &= |\langle \mathbf{Q}_1 | e^{-\beta\hat{H}/2} | G(\mathbf{Q}_0, \mathbf{P}_0) \rangle|^2. \quad (2.45)
 \end{aligned}$$

### III. APPLICATION TO LIQUID *para*-HYDROGEN

#### A. Interaction potential between *para*-hydrogen molecules

Our calculations employ the Silvera–Goldman potential.<sup>89</sup> This potential has been used widely in quantum simulations of liquid *para*-hydrogen to study thermodynamic properties, transport, and density fluctuations. The results of such Monte Carlo path integral calculations<sup>84</sup> using this potential are in very good agreement with experimental data.

In the Silvera–Goldman potential the H<sub>2</sub> molecule is treated as a spherical particle. As a result, potential interactions between H<sub>2</sub> molecules in liquid *para*-hydrogen depend only on the distance between them, allowing application of the PP-FBSD methodology described in the previous section. The spherical approximation is known to be very accurate at

TABLE I. Parameters of the Silvera–Goldman potential for *para*-hydrogen molecule. All values are in atomic units.

Parameter	Value (atomic units)
$\alpha$	1.713
$\beta$	1.5671
$\gamma$	0.009 93
$C_6$	12.14
$C_8$	215.2
$C_{10}$	4813.9
$C_9$	143.1
$r_c$	8.321

temperatures lower than the rotational temperature of H<sub>2</sub> molecule ( $T = 85$  K). The H<sub>2</sub> molecule is considered to be in its rotational ground state ( $J = 0$ ) at the temperature of the present study.

The Silvera–Goldman potential has the form

$$\begin{aligned}
 V(r) &= \exp(\alpha - \delta r - \gamma r^2) \\
 &- \left( \frac{C_6}{r^6} + \frac{C_8}{r^8} + \frac{C_{10}}{r^{10}} \right) f_c(r) + \frac{C_9}{r^9} f_c(r), \quad (3.1)
 \end{aligned}$$

where

$$f_c(r) = \begin{cases} e^{-(r_c/r - 1)^2} & (r \leq r_c) \\ 1 & (r > r_c). \end{cases} \quad (3.2)$$

The first term on the right-hand side in Eq. (3.1) corresponds to short-range repulsive interactions, while the second one describes long-range attractive interactions. The last term is an effective two-body approximation to the three-body Axelrod–Teller–Muto triple dipole dispersion interaction. The function  $f_c(r)$  is used to damp the effects of attractive interactions at short distances. The potential has a well depth of 31.7 K at the minimum, which occurs at 3.44 Å. The values of parameters used in the interaction potential are listed in Table I.

#### B. Computational details

Since the interaction between *para*-hydrogen molecules is assumed to be isotropic, we use the same value for the coherent state parameter  $\gamma$  for all degrees of freedom involved.

The calculations were performed under minimum image periodic boundary conditions, where each cell consists of 108 *para*-hydrogen molecules, at several thermodynamic state points between  $T = 25$  K (a high temperature liquid, with molar volume  $v = 31.7$  cm<sup>3</sup> mol<sup>-1</sup>) and  $T = 14$  K (a liquid near the triple point,  $v = 25.6$  cm<sup>3</sup> mol<sup>-1</sup>). These values are taken from the results of the path integral Monte Carlo calculations under roughly zero external pressure<sup>85</sup> and are summarized in Table II. The results were obtained using two (at  $T = 25$  K) to five (at  $T = 14$  K) million trajectories. The equations of motion for classical trajectories were solved us-

TABLE II. Kinetic energies and molar volume of liquid *para*-hydrogen under nearly zero external pressure. The values of molar volume are taken from Ref. 84.

Temperature (K)	Kinetic Energy (K/particle)			Molar volume (cm <sup>3</sup> mol <sup>-1</sup> )	
	Pair-product	PIMC	Classical	PIMC	Classical
14	68.6	63.2	21.0	25.6	16.6
17	66.5	62.0	25.5	26.9	17.0
20	65.1	62.0	30.0	28.1	17.3
25	64.0	61.9	37.5	31.7	20.2

ing the velocity Verlet algorithm<sup>90</sup> with a time step of 0.5 fs. All calculations were performed on a PC cluster configured with 16 nodes.

Standard imaginary time path integral Monte Carlo (PIMC) calculations were also performed under the same conditions in order to assess the accuracy of the single-bead pair-product approximation employed in the FBSD scheme. The Trotter factorization was used for a short-time propagator and the number of slices was chosen large enough to yield converged results (e.g.,  $N=30$  at  $T=25$  K and  $N=50$  at  $T=14$  K).

### C. Results and discussion

First we examine the accuracy of the pair-product approximation by comparing the expectation value of the kinetic energy at  $t=0$  with that obtained by the PIMC calculations. The expectation value of the kinetic energy can be obtained simply by setting  $\hat{A} = \hat{p}/2m$ ,  $\hat{B} = \hat{p}$ . The calculated results using  $\gamma=1.5$  a.u. are shown in Fig. 1 (see also Table II), along with that of numerically exact PIMC calculations and the corresponding classical estimates ( $1.5k_B T$ ). In the case of high temperature, one observes a good agreement with the PIMC results. This pair-product approximation tends to overestimate the kinetic energy as the system temperature decreases. Considering that we use a single imagi-

nary time step that is well over an order of magnitude larger than that employed in the PIMC calculations, this agreement is satisfactory. It is seen that the dependence of the kinetic energy on temperature is very small, indicating that zero-point energy is dominant under these conditions. The coherent state density is described reasonably well by the pair-product form, and quantum effects such as zero-point energy are adequately accounted for.

Next, we investigate the pair distribution function  $g(r)$  by setting

$$\hat{A} = 1, \quad \hat{B} = \frac{v}{n^2} \sum_{i < j}^n \delta(r - |\hat{\mathbf{r}}^{(i)} - \hat{\mathbf{r}}^{(j)}|). \quad (3.3)$$

Figure 2 shows the *para*-hydrogen (center-of-mass) pair distribution function along with that of the PIMC calculation and the classical one at  $T=25$  K ( $v=31.7$  cm<sup>3</sup> mol<sup>-1</sup>). The classical calculation is performed under zero external pressure with the thermodynamic parameters shown in Table II. As is clearly seen, quantum effects are prominent, and the quantum calculation exhibits decreased spatial ordering. The distribution function in the pair-product approximation shows very good agreement with the PIMC calculation. Figure 3 displays the results of quantum calculations at  $T=14$  K ( $v=25.6$  cm<sup>3</sup> mol<sup>-1</sup>). At this temperature, classical

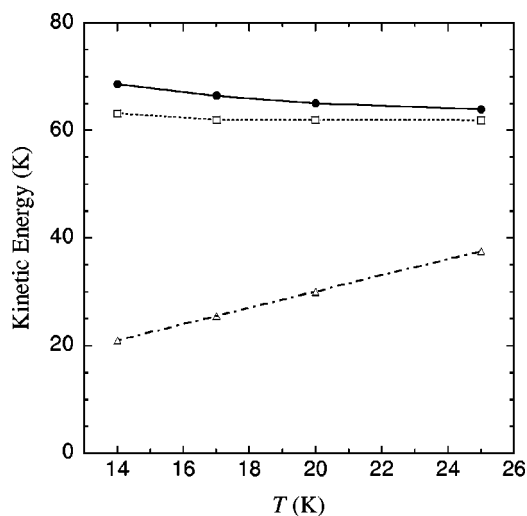


FIG. 1. Kinetic energy as a function of temperature for liquid *para*-hydrogen from  $T=14$  K to  $T=25$  K. Solid circles: Results by the pair-product approximation for the coherent state density. Hollow squares: Path integral Monte Carlo calculations. Hollow triangles: Classical estimates ( $1.5k_B T$ ).

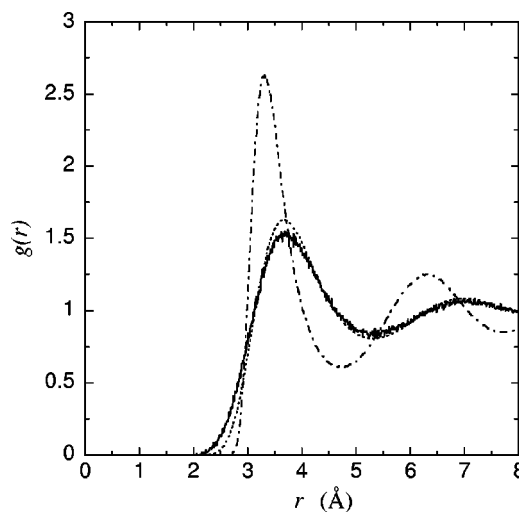


FIG. 2. The *para*-hydrogen (center-of-mass) pair distribution function for liquid *para*-hydrogen at  $T=25$  K under nearly zero external pressure. Solid line: Result by the pair-product approximation for the coherent state density ( $v=31.7$  cm<sup>3</sup> mol<sup>-1</sup>). Dotted line: Path integral Monte Carlo calculation ( $v=31.7$  cm<sup>3</sup> mol<sup>-1</sup>). Dot-dashed line: Classical result ( $v=20.2$  cm<sup>3</sup> mol<sup>-1</sup>).

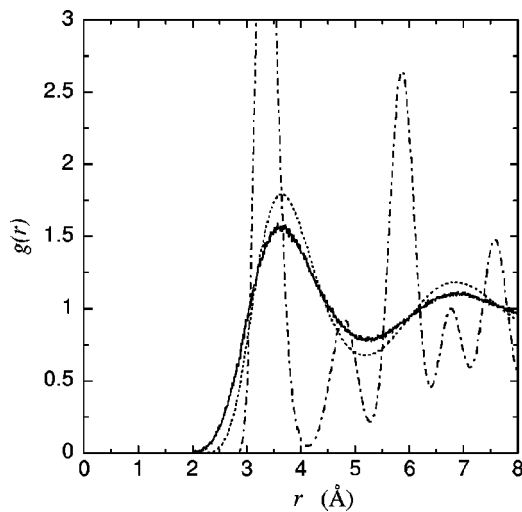


FIG. 3. The *para*-hydrogen (center-of-mass) pair distribution function for liquid *para*-hydrogen at  $T=14$  K under nearly zero external pressure. Solid line: Result by the pair-product approximation for the coherent state density ( $v=25.6$  cm<sup>3</sup> mol<sup>-1</sup>). Dotted line: Path integral Monte Carlo calculation ( $v=25.6$  cm<sup>3</sup> mol<sup>-1</sup>). Dot-dashed line: Classical result ( $v=16.6$  cm<sup>3</sup> mol<sup>-1</sup>).

simulation predicts that *para*-hydrogen is in an ordered solid state, rather than liquid, and several peaks are observed in the distribution function in Fig. 3. Compared with the  $T=25$  K results, agreement with the exact PIMC result becomes somewhat worse and the distribution function in the pair-product approximation is slightly less structured, but still good overall agreement is obtained. This discrepancy from the PIMC result at low temperature is also seen in the calculation of the kinetic energy and can be attributed mainly to the neglect of three- and higher-body correlations. The pair-product form can be regarded as the lowest order density expansion of the coherent state density matrix elements and causes a substantial error when three or more particles are in close proximity. This probability depends on the density.

Finally, we comment on the choice of the coherent state parameter  $\gamma$ . The optimal choice of this parameter is not entirely straightforward, in particular in the case of liquids. A reasonable value can be inferred from the harmonic frequency around the equilibrium internuclear distance using the relation  $\gamma=m\omega/2\hbar$ . There is ample evidence that values of the coherent state parameter in the range suggested by this relation minimize the error in the coherent state representation of the semiclassical propagator.<sup>24,25,38,83</sup> In a linear configuration where three *para*-hydrogen molecules are placed at intervals equal to the equilibrium nuclear distance the above formula gives approximately  $\gamma=0.52$  a.u. for the central molecule by using this effective harmonic frequency.

In the pair-product approximation, the effective potential  $u(\mathbf{r}, \mathbf{r}_0, \mathbf{p}_0)$  depends on the coherent state parameter  $\gamma$  as well as the imaginary time step  $\tau$ . As a result, there is dependence on  $\gamma$  even in calculated static properties (at  $t=0$ ). To clarify this, we examined the dependence of the kinetic energy on the coherent state parameter  $\gamma$  and found that stable results are obtained for  $\gamma \geq 1.5$  a.u. (These converged results are shown in Fig. 1 and Table II.) As  $\gamma$  is decreased the kinetic energy increases and agreement with the PIMC calculations

becomes worse. A similar trend is observed in the calculation of the pair distribution function  $g(r)$ . The sensitivity of the results to  $\gamma$  is more pronounced at lower temperatures than at higher temperatures.

The accuracy of the pair-product approximation depends roughly on the coefficient  $m\gamma/(m+2\hbar^2\tau\gamma)$ , which appears in the exponent of the matrix element of a free-particle [see Eq. (2.17) with the replacement  $\tau=\Delta\beta/2$ ], in a similar manner that the quality of the short time propagator is determined by its time step. This can be rationalized if we consider the Gaussian part of the coherent state representation as an imaginary-time propagation and the above coefficient is given as a combined propagation of an imaginary time  $\tau$  and an additional one originating from the coherent state representation. Therefore, the pair-product approximation becomes more accurate as the above coefficient increases in the same way as the short time propagator becomes more accurate with a shorter time step. Also, considering that the effective potential  $u(\mathbf{r}, \mathbf{r}_0, \mathbf{p}_0)$  approaches  $\tau V(\mathbf{r})$  in the high temperature limit, the approximation becomes more accurate as  $\tau$  is decreased when  $\gamma$  is fixed. These considerations are completely consistent with the obtained results. The stable results obtained with  $\gamma \geq 1.5$  a.u. are, therefore, reasonably accurate.

Another consideration concerning the choice of  $\gamma$  is sampling efficiency. Small values of the coherent state parameter lead to numerical problems, as the force constant associated with the springs that connect  $\mathbf{r}_0$  with the path integral bead  $\mathbf{r}_1$  becomes small. This is seen most transparently from the Trotter-discretized path integral representation of the FBSD expression. The presence of the Boltzmann factor  $\exp(-\Delta\beta V(\mathbf{r}_1^{(1)}, \mathbf{r}_1^{(2)}, \dots))$  guarantees that the path integral beads of different atoms remain sufficiently far from one another due to repulsive interactions. Since the coherent state variable  $\mathbf{r}_0$  is not subject to the system potential, special care must be taken to limit the space accessed by this variable to the vicinity of  $\mathbf{r}_1$ . By forcing  $\mathbf{r}_0^{(i)}$  to remain close to  $\mathbf{r}_1^{(i)}$  for each atom one ensures that the coordinates  $\mathbf{r}_0^{(1)}, \mathbf{r}_0^{(2)}, \dots, \mathbf{r}_0^{(n)}$  (which define the system configuration at the start of a classical trajectory) are well separated, avoiding unphysical initial conditions corresponding to near-collision events. These arguments apply qualitatively to the PP representation of the coherent state density.

Finally, as argued in Sec. II B, large values of the coherent state parameter lead to the sampling of unfavorably large momentum values and are to be avoided. In the present case we have found the value  $\gamma=1.5$  a.u. was sufficiently large to avoid the sampling of unphysical arrangements of the H<sub>2</sub> molecules but not too large to lead to the selection of extremely large momentum values. The results of our simulations were insensitive to an increase of the coherent parameter by a factor of two.

Figure 4 shows the normalized velocity autocorrelation function obtained at  $T=25$  K. The real part of the correlation function exhibits a smooth and monotonic decay without negative parts. The correlation function obtained via classical calculations<sup>91,92</sup> (not shown) decays much faster and has a minimum around 0.17 ps with a depth of about 15% of the maximum value at  $t=0$ . As can be seen in the figure, the

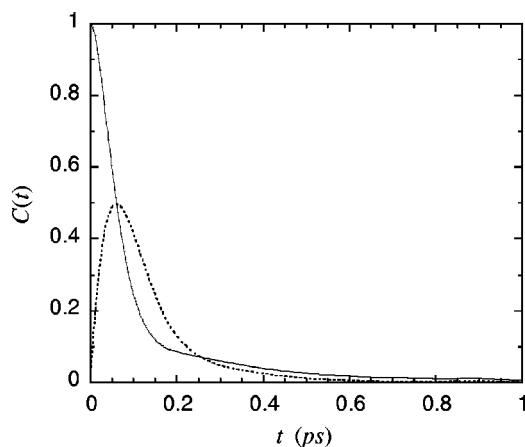


FIG. 4. The normalized velocity autocorrelation function of liquid *para*-hydrogen at  $T=25$  K ( $v=31.7$  cm<sup>3</sup> mol<sup>-1</sup>), calculated by the PP-FBSD method. The solid and dotted lines are the real and imaginary parts of the correlation function, respectively.

maximum of the imaginary component amounts to about half of the maximum value of the real component at  $t=0$ , which clearly indicates the quantum nature of liquid *para*-hydrogen at  $T=25$  K. We find that both the real and imaginary parts of the correlation function are in very good agreement with those obtained by the quantum mode-coupling approach.<sup>77</sup> The correlation function obtained by the centroid molecular dynamics (CMD) method<sup>91,93</sup> decays somewhat faster in comparison to the PP-FBSD result.

We have calculated the diffusion constant according to the following Green–Kubo relation:<sup>94</sup>

$$D = \frac{1}{3m^2n} \int_0^\infty \text{Re } C_{\mathbf{p},\mathbf{p}}(t) dt. \quad (3.4)$$

The calculated value of the diffusion constant by the FBSD method is  $1.68$  Å<sup>2</sup>/ps, in excellent agreement with the experimental value of  $1.6$  Å<sup>2</sup>/ps and other theoretical calculations (see Table III). Again the classical prediction is  $0.5$  Å<sup>2</sup>/ps, more than three times smaller than the PP-FBSD.

At  $T=14$  K the correlation function (shown in Fig. 5) decays faster and has a prominent negative part. The initial decay at short time until it crosses zero ( $\sim 0.1$  ps) is in good agreement with the results of quantum mode-coupling approach and the maximum entropy analytic continuation method.<sup>78</sup> This agreement is to be expected, since all three of

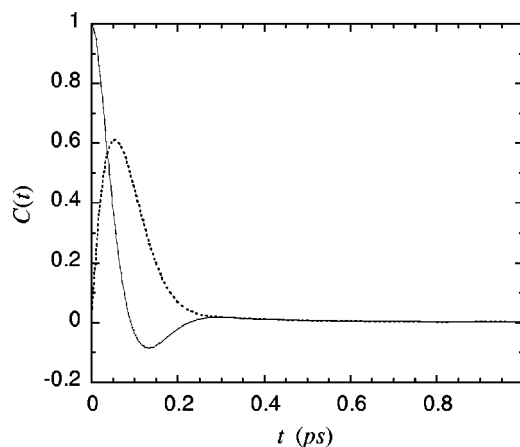


FIG. 5. The normalized velocity autocorrelation function of liquid *para*-hydrogen at  $T=14$  K ( $v=25.6$  cm<sup>3</sup> mol<sup>-1</sup>), calculated by the PP-FBSD method. The solid and dotted lines are the real and imaginary parts of the correlation function, respectively.

these methods involve approximations that are particularly well-justified at short time; specifically, the quantum mode-coupling theory is exact to order  $t^6$ ; the statistical error in the maximum entropy analytic continuation method is small at times near zero; and the quality of the PP-FBSD result at  $t=0$  depends on the error of the single-bead PP approximation, which was seen to be very small. The position and depth of the first minimum in the correlation function differ slightly from that obtained in the quantum mode-coupling approach and the maximum entropy analytic continuation method. The position of the first minimum by the FBSD method is rather close to the results of the CMD method.<sup>93</sup> The maximum of the imaginary component is higher, reaching a height equal to about 60% of the maximum of the real part at  $t=0$ . This magnitude is consistent with the results of quantum mode-coupling approach. Classical simulations predict that *para*-hydrogen is in a nondiffusive ordered solid state. Therefore, a comparison with classical results cannot be made at this temperature. The calculated diffusion constant by the FBSD method is relatively large ( $0.75$  Å<sup>2</sup>/ps), compared to experiments and other theoretical calculations. This can be attributed primarily to the relatively small contribution of the negative part of the correlation function, in addition to its higher value at  $t=0$ , which arises from the small overestimation of the kinetic energy by the single-bead PP approximation.

Figure 6 shows the diffusion constant as a function of temperature, along with experimentally measured values.<sup>68</sup> In the high temperature limit where a system is expected to be nearly classical it has been shown that the result of the FBSD method agrees with that of a purely classical treatment.<sup>53</sup> This observation appears to remain valid in a regime where quantum effects become quite sizable, as long as the coherent state density is evaluated with sufficient accuracy. Below  $T=20$  K the single-bead PP-FBSD results show a larger deviation from the experimental values. These differences are likely to arise from the less accurate description of the density offered by the single-bead PP approximation when applied with a larger imaginary time step. Still, the

TABLE III. Diffusion constant for liquid *para*-hydrogen at  $T=14$  K and  $T=25$  K under nearly zero external pressure.

	Diffusion constant (Å <sup>2</sup> /ps)	
	$T=14$ K	$T=25$ K
PP-FBSD	$0.75 \pm 0.07$	$1.68 \pm 0.05$
Quantum mode-coupling method (Ref. 77)	0.30	1.69
Maximum entropy analytic continuation method (Ref. 78)	0.28	1.47
Centroid MD (Ref. 93)	0.32	1.54
Classical MD (Ref. 93)	Solid	0.5
Experiment (Ref. 68)	0.4	1.6

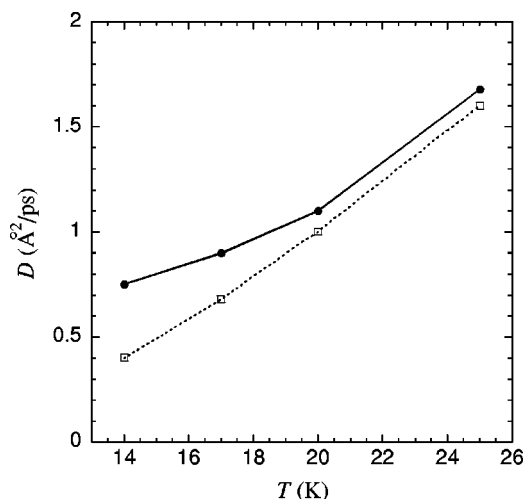


FIG. 6. The diffusion constant as a function of temperature for liquid *para*-hydrogen from  $T=14$  K to  $T=25$  K. Solid circles: PP-FBSD results. Hollow squares: Experimental results.

correct trends are observed, and the single-bead PP-FBSD method is at least semiquantitative at these low temperatures.

Since liquid *para*-hydrogen is very dense at  $T=14$  K (close to the triple-point), treatment of the coherent state density by the single-bead PP form is not adequate. Three- (and higher-) body correlations play an important role in this case. More accurate results could be obtained by employing more than one PP bead in the path integral representation of the Boltzmann operator, or by including three-body correlation for the coherent state density. Explicit construction of this term as a function of all coordinates of three-particles may be possible, but much more difficult and less practical. One may be able to include this correlation effectively by using some simple “polarizability” form.

#### IV. CONCLUDING REMARKS

We have developed a FBSD methodology that uses a pair-product approximation of the coherent state density. The PP-FBSD formulation corresponds to the rigorous stationary phase limit of the time correlation function with an accurate quantum mechanical representation of the Boltzmann operator based on a superior imaginary time propagator. Even in the limit of a single path integral bead, this representation leads to a faithful representation of the low-temperature coherent state density and thus allows simulation of quantum fluids with hundreds of atoms. This method has been applied to quantum self-diffusion in liquid *para*-hydrogen, where the calculated results were in excellent agreement with experimental values and other theoretical approximations at temperatures higher than 20 K. The diffusion constant obtained by the PP-FBSD method deviates somewhat from the experimental value as the temperature of the system decreases further due to the deterioration of the single-bead PP approximation.

As discussed in Sec. II, the PP-FBSD approximation is not restricted to the use of a single path integral bead. In the primitive (Trotter) discretization of the FBSD correlation function phase cancellation, in conjunction with the high di-

mension of the multi-bead path integral expression, prohibits convergence in condensed phase systems. The severity of phase cancellation in the path integral representation of the coherent state density with multiple beads depends on the coherent state parameter  $\gamma$  and the imaginary time step  $\Delta\beta$ . The PP approximation allows the use of a much larger imaginary time step compared to the primitive Trotter form and thus phase cancellation can be diminished to a large extent. This fact, along with the dramatic reduction of dimension achieved by the more accurate PP propagator, extends the feasibility of FBSD calculations to much larger systems.

An accurate and practical (i.e., without severe phase cancellation) treatment of the coherent state density is an important component of the FBSD procedure in order to be applicable to large quantum systems at finite temperature. The present PP development makes the FBSD method one of the most practical and versatile methods for obtaining a quantitative description of chemical dynamics in low-temperature quantum fluids.

#### ACKNOWLEDGMENTS

This work was supported by the National Science Foundation under award No. CHE-0212640. We thank Dr. Nicholas J. Wright for useful discussions regarding the application of the Trotter-discretized path integral FBSD method to liquid *para*-hydrogen.

- <sup>1</sup>R. P. Feynman, *Rev. Mod. Phys.* **20**, 367 (1948).
- <sup>2</sup>R. P. Feynman and A. R. Hibbs, *Quantum Mechanics and Path Integrals* (McGraw-Hill, New York, 1965).
- <sup>3</sup>V. S. Filinov, *Nucl. Phys. B* **271**, 717 (1986).
- <sup>4</sup>N. Makri and W. H. Miller, *Chem. Phys. Lett.* **139**, 10 (1987).
- <sup>5</sup>N. Makri, *Comput. Phys. Commun.* **63**, 389 (1991).
- <sup>6</sup>J. D. Doll, D. L. Freeman, and T. L. Beck, *Adv. Chem. Phys.* **78**, 61 (1990).
- <sup>7</sup>*Quantum Monte Carlo Methods in Condensed Matter Physics*, edited by M. Suzuki (World Scientific, Singapore, 1993).
- <sup>8</sup>J. H. Van Vleck, *Proc. Natl. Acad. Sci. U.S.A.* **14**, 178 (1928).
- <sup>9</sup>C. Morette, *Phys. Rev.* **81**, 848 (1952).
- <sup>10</sup>M. P. Allen and D. J. Tildesley, *Computer Simulations of Liquids* (Oxford University Press, Oxford, 1987).
- <sup>11</sup>W. H. Miller, *Adv. Chem. Phys.* **25**, 69 (1974).
- <sup>12</sup>W. H. Miller, *Adv. Chem. Phys.* **30**, 77 (1975).
- <sup>13</sup>E. J. Heller, *Acc. Chem. Res.* **14**, 368 (1981).
- <sup>14</sup>M. S. Child, *Semiclassical Mechanics with Molecular Applications* (Clarendon, Oxford, 1991).
- <sup>15</sup>W. H. Miller, *J. Chem. Phys.* **53**, 3578 (1970).
- <sup>16</sup>M. F. Herman and E. Kluk, *Chem. Phys.* **91**, 27 (1984).
- <sup>17</sup>E. Kluk, M. F. Herman, and H. L. Davis, *J. Chem. Phys.* **84**, 326 (1986).
- <sup>18</sup>E. J. Heller, *J. Chem. Phys.* **94**, 2723 (1991).
- <sup>19</sup>W. H. Miller, *J. Chem. Phys.* **95**, 9428 (1991).
- <sup>20</sup>W. H. Miller, *Faraday Discuss.* **110**, 1 (1998).
- <sup>21</sup>G. Campolieti and P. Brumer, *Phys. Rev. A* **50**, 997 (1994).
- <sup>22</sup>J. Wilkie and P. Brumer, *Phys. Rev. A* **61**, 064101 (2001).
- <sup>23</sup>K. G. Kay, *J. Chem. Phys.* **100**, 4377 (1994).
- <sup>24</sup>K. G. Kay, *J. Chem. Phys.* **100**, 4432 (1994).
- <sup>25</sup>K. G. Kay, *J. Chem. Phys.* **107**, 2313 (1997).
- <sup>26</sup>A. R. Walton and D. E. Manolopoulos, *Mol. Phys.* **87**, 961 (1996).
- <sup>27</sup>W. H. Miller, *J. Phys. Chem.* **105**, 2942 (2001).
- <sup>28</sup>M. A. Sepulveda and F. Grossmann, *Adv. Chem. Phys.* **XCVI**, 191 (1996).
- <sup>29</sup>D. J. Tannor and S. Garashchuk, *Annu. Rev. Phys. Chem.* **51**, 553 (2000).
- <sup>30</sup>M. L. Brewer, J. S. Hulme, and D. E. Manolopoulos, *J. Chem. Phys.* **106**, 4832 (1997).
- <sup>31</sup>S. Garashchuk, F. Grossmann, and D. Tannor, *J. Chem. Soc., Faraday Trans.* **93**, 781 (1997).
- <sup>32</sup>X. Sun and W. H. Miller, *J. Chem. Phys.* **106**, 6346 (1997).
- <sup>33</sup>X. Sun and W. H. Miller, *J. Chem. Phys.* **108**, 8870 (1998).

- <sup>34</sup>V. Guallar, V. S. Batista, and W. H. Miller, *J. Chem. Phys.* **110**, 9922 (1999).
- <sup>35</sup>M. Thoss, W. H. Miller, and G. Stock, *J. Chem. Phys.* **112**, 10282 (2000).
- <sup>36</sup>E. A. Coronado, V. S. Batista, and W. H. Miller, *J. Chem. Phys.* **112**, 5566 (2000).
- <sup>37</sup>M. Ovchinnikov, V. A. Apkarian, and G. A. Voth, *J. Chem. Phys.* **114**, 7130 (2001).
- <sup>38</sup>T. Yamamoto and W. H. Miller, *J. Chem. Phys.* **118**, 2135 (2003).
- <sup>39</sup>H. Wang, D. E. Manolopoulos, and W. H. Miller, *J. Chem. Phys.* **115**, 6317 (2001).
- <sup>40</sup>T. Yamamoto, H. Wang, and W. H. Miller, *J. Chem. Phys.* **116**, 7335 (2002).
- <sup>41</sup>N. Makri and K. Thompson, *Chem. Phys. Lett.* **291**, 101 (1998).
- <sup>42</sup>K. Thompson and N. Makri, *J. Chem. Phys.* **110**, 1343 (1999).
- <sup>43</sup>K. Thompson and N. Makri, *Phys. Rev. E* **59**, R4729 (1999).
- <sup>44</sup>X. Sun and W. H. Miller, *J. Chem. Phys.* **110**, 6635 (1999).
- <sup>45</sup>J. Shao and N. Makri, *J. Phys. Chem.* **103**, 7753 (1999).
- <sup>46</sup>J. Shao and N. Makri, *J. Phys. Chem.* **103**, 9479 (1999).
- <sup>47</sup>O. Kühn and N. Makri, *J. Phys. Chem.* **103**, 9487 (1999).
- <sup>48</sup>J. Shao and N. Makri, *J. Chem. Phys.* **113**, 3681 (2000).
- <sup>49</sup>E. Jezek and N. Makri, *J. Phys. Chem.* **105**, 2851 (2001).
- <sup>50</sup>N. Makri, in *Fluctuating Paths and Fields*, edited by W. Janke, A. Pelster, H.-J. Schmidt, and M. Bachmann (World Scientific, Singapore, 2001).
- <sup>51</sup>N. Makri and J. Shao, in *Accurate Description of Low-Lying Electronic States and Potential Energy Surfaces*, edited by M. Hoffmann (Oxford University Press, 2002).
- <sup>52</sup>N. Makri, *J. Phys. Chem. B* **106**, 8390 (2002).
- <sup>53</sup>N. J. Wright and N. Makri, *J. Chem. Phys.* **119**, 1634 (2003).
- <sup>54</sup>V. S. Batista, M. T. Zanni, J. Greenblatt, D. M. Neumark, and W. H. Miller, *J. Chem. Phys.* **110**, 3736 (1999).
- <sup>55</sup>D. E. Skinner and W. H. Miller, *J. Chem. Phys.* **111**, 10787 (1999).
- <sup>56</sup>H. Wang, M. Thoss, and W. H. Miller, *J. Chem. Phys.* **112**, 47 (2000).
- <sup>57</sup>M. Thoss, H. Wang, and W. H. Miller, *J. Chem. Phys.* **114**, 9220 (2001).
- <sup>58</sup>R. Gelabert, X. Giménez, M. Thoss, H. Wang, and W. H. Miller, *J. Chem. Phys.* **114**, 2572 (2001).
- <sup>59</sup>H. Wang, M. Thoss, K. L. Sorge, R. Gelabert, X. Giménez, and W. H. Miller, *J. Chem. Phys.* **114**, 2562 (2001).
- <sup>60</sup>E. J. Wigner, *Chem. Phys.* **5**, 720 (1937).
- <sup>61</sup>E. J. Heller, *J. Chem. Phys.* **65**, 1289 (1976).
- <sup>62</sup>H. Wang, X. Sun, and W. H. Miller, *J. Chem. Phys.* **108**, 9726 (1998).
- <sup>63</sup>R. Hernandez and G. A. Voth, *Chem. Phys.* **233**, 243 (1998).
- <sup>64</sup>N. Makri and W. H. Miller, *J. Chem. Phys.* **116**, 9207 (2002).
- <sup>65</sup>R. P. Feynman, *Statistical Mechanics* (Addison-Wesley, Redwood City, 1972).
- <sup>66</sup>D. M. Ceperley and E. L. Pollock, *Phys. Rev. Lett.* **56**, 351 (1986).
- <sup>67</sup>D. M. Ceperley, *Rev. Mod. Phys.* **67**, 279 (1995).
- <sup>68</sup>B. N. Esel'son, Y. P. Blagoi, V. V. Grigor'ev, V. G. Manzhelii, S. A. Mikhailenko, and N. P. Neklyudov, *Properties of Liquid and Solid Hydrogen* (Israel Program for Scientific Translations, Jerusalem, 1971). Translated from the Russian by Ch. Niesenbaum.
- <sup>69</sup>F. J. Bermejo, B. Fak, S. M. Bennington, R. Fernandez-Perea, C. Cabrillo, J. Dawidowski, M. T. Fernandez-Diaz, and P. Verkerk, *Phys. Rev. B* **60**, 15154 (1999).
- <sup>70</sup>F. J. Bermejo, K. Kinugawa, C. Cabrillo, S. M. Bennington, B. Fak, M. T. Fernandez-Diaz, P. Verkerk, J. Dawidowski, and R. Fernandez-Perea, *Phys. Rev. Lett.* **84**, 5359 (2000).
- <sup>71</sup>J. Cao and G. J. Martyna, *J. Chem. Phys.* **104**, 2028 (1996).
- <sup>72</sup>M. Pavese and G. A. Voth, *Chem. Phys. Lett.* **249**, 231 (1996).
- <sup>73</sup>A. Calhoun, M. Pavese, and G. A. Voth, *Chem. Phys. Lett.* **262**, 415 (1996).
- <sup>74</sup>K. Kinugawa, *Chem. Phys. Lett.* **292**, 454 (1998).
- <sup>75</sup>G. J. Martyna, A. Hughes, and M. Tuckerman, *J. Chem. Phys.* **110**, 3275 (1999).
- <sup>76</sup>E. Rabani and D. R. Reichman, *J. Chem. Phys.* **116**, 6271 (2002).
- <sup>77</sup>D. R. Reichman and E. Rabani, *J. Chem. Phys.* **116**, 6279 (2002).
- <sup>78</sup>E. Rabani, D. R. Reichman, G. Krilov, and B. J. Berne, *Proc. Natl. Acad. Sci. U.S.A.* **99**, 1129 (2002).
- <sup>79</sup>B. J. Berne and G. D. Harp, *Adv. Chem. Phys.* **17**, 63 (1970).
- <sup>80</sup>R. J. Glauber, *Phys. Rev.* **130**, 2529 (1963).
- <sup>81</sup>M. F. Trotter, *Proc. Am. Math. Soc.* **10**, 545 (1959).
- <sup>82</sup>D. Chandler and P. G. Wolynes, *J. Chem. Phys.* **74**, 4078 (1981).
- <sup>83</sup>N. J. Wright and N. Makri (unpublished).
- <sup>84</sup>D. J. Scharf, G. J. Martyna, and M. L. Klein, *Low Temp. Phys.* **19**, 364 (1993).
- <sup>85</sup>N. Makri and W. H. Miller, *Chem. Phys. Lett.* **151**, 1 (1988).
- <sup>86</sup>R. D. Coalson, D. L. Freeman, and J. D. Doll, *J. Chem. Phys.* **91**, 4242 (1989).
- <sup>87</sup>P. Zhang, R. M. Levy, and R. A. Friesner, *Chem. Phys. Lett.* **144**, 236 (1988).
- <sup>88</sup>N. Makri, *Chem. Phys. Lett.* **193**, 435 (1992).
- <sup>89</sup>I. F. Silvera and V. V. Goldman, *J. Chem. Phys.* **69**, 4209 (1978).
- <sup>90</sup>W. C. Swope, H. C. Andersen, P. H. Berens, and K. R. Wilson, *J. Chem. Phys.* **76**, 637 (1982).
- <sup>91</sup>J. Cao and G. J. Martyna, *J. Chem. Phys.* **104**, 2028 (1996).
- <sup>92</sup>M. Pavese and G. A. Voth, *Chem. Phys. Lett.* **249**, 231 (1996).
- <sup>93</sup>A. Calhoun, M. Pavese, and G. A. Voth, *Chem. Phys. Lett.* **262**, 415 (1996).
- <sup>94</sup>R. Kubo, M. Toda, and N. Hashitsume, *Statistical Physics*, 2nd ed. (Springer-Verlag, Heidelberg, 1991).